ASIA-PACIFIC JOURNAL OF CHEMICAL ENGINEERING
Asia-Pac. J. Chem. Eng. 2009; **4**: 55–67
Published online 13 October 2008 in Wiley InterScience
(www.interscience.wiley.com) DOI:10.1002/apj.195

Special Theme Research Article

Numerical model for polymer electrolyte membrane fuel cells with experimental application and validation

Javier Alonso Mora, Attila P., Husar, Maria Serra and Jordi Riera*

Institute of Robotics and Industrial Informatics at Barcelona IRI (CSIC-UPC), Spain

Received 18 January 2008; Revised 3 March 2008; Accepted 21 May 2008

ABSTRACT: The aim of this paper is to present a simple 3D computational model of a polymer electrolyte membrane fuel cell (PEMFC) that simulates over time the heat distribution, energy, and mass balance of the reactant gas flows in the fuel cell including pressure drop, humidity, and liquid water. Although this theoretical model can be adapted to any type of PEMFC, for verification of the model and to present different analysis it has been adapted to a single cell test fixture. The model parameters were adjusted through a series of experimental tests and the model was experimentally validated for a well-defined range of operating conditions: H_2/air O_2 as reactants, flow rates of 0.5–1.5 SLPM, dew points and cell temperatures of 30–80 °C, currents 0–5 A and with/without water condensation. The model is especially suited for the analysis of liquid water condensation in the reactant channels. A key finding is that the critical current at which liquid water is formed is determined at different flows, temperatures, and humidity. © 2008 Curtin University of Technology and John Wiley & Sons, Ltd.

KEYWORDS: numerical modeling; PEM fuel cell; temperature distribution; pressure drop; parameter identification; experimental validation

INTRODUCTION

Polymer electrolyte membrane fuel cells (PEMFCs) have tremendous potential as energy conversion devices for a wide range of applications. However, there is a great deal to be learnt about the various interactions between the different physical phenomena that occur in the fuel cell. There are a vast number of studies in the literature that model the fuel cells with varying degrees of complexity. However most of them do not validate their model with experimental data. Static models, in particular, saw an important evolution in the 1990s. For instance, isothermal conditions are assumed by many authors such as Springer *et al*. (1991),[1] while others include thermal distribution (Nguyen, 1993)[2]. Spatial variation in only one dimension was considered initially (Springer, 1991)[1] while variation in two[17] and three dimensions was introduced later (Broka, 1997)[3] (Coppo, 2006)[4]. Some works do not model the two phases of water while others do (Bernardi, 1992)[5,15].

Dynamic models of physics and control solutions for PEMFC have evolved greatly in the past decade. However, the majority of these dynamic models have a low level of detail. Very few dynamic studies include essential characteristics, such as temperature distribution, formation of liquid water in different zones of the fuel cell, or pressure drop along the channels. Shan (2005)[6] and Um (2006)[7] present very complete models with heat distribution but their works do not take liquid water into account.

This study presents a dynamic model for PEMFC, which includes the computation of the thermal properties and temperature distribution of the fuel cell and the pressure drop in the reactant gases while taking into account the condensation of water, as well as the resulting effects on the flow and pressure fields. The experimental tests for parameter identification are described. The model is based on the numerical solution of heat transfer problems expressed as various equilibrium differential equations, using numerical iterative methods. In the section on Description of the Model, the model is described; sections on Application of the Model to a Single Cell Test Fixture and Experimental Methodology explain the application of the model to a specific single cell and the experimental methodology for the parameter identification and model validation; the section on Selected Results for the Single Cell Test Fixture collects the principal simulation results and emphasizes the features of the model. The main conclusions are summarized in the section on Conclusions.

**Correspondence to*: Maria Serra, Institute of Robotics and Industrial Informatics at Barcelona IRI (CSIC-UPC), Spain.
E-mail: maserra@iri.upc.edu

DESCRIPTION OF THE MODEL

The anode and cathode reactants are modeled separately from the stack and interact with it through convection heat transfer in the channels.[8] The pressure drop in the channels is experimentally determined using major and minor losses (for laminar flows).[9] Water and heat created inside the fuel cell due to the reaction are determined by commonly used equations which are explained in the section on Heat Transfer (Thermal Generation) at the Active Area and the section on Heat Transfer at the Channels and Active Area due to Reactant Flows.[10]

The model can be conceived as two submodels working together, a thermal and a pressure drop (the analytical nature of the thermal equation).

Thermal model

The thermal equilibrium equation (thermal generation plus heat transfer equal to energy stored per second) can be approximately solved by creating a mesh of the fuel cell, assuming constant temperature in each cuboid inside the mesh. Iterating with an adequate time interval, each cuboid is represented by a node situated at its midpoint. A correct mesh is crucial to obtain good results. As an example, the mesh used in our case is shown in the section on Model Assumptions (Fig. 2).

In this work, the following finite differences method is used for the simulation of the temperature field:

$$T_i^{k+1} = \frac{\Delta t}{C_i}\left[\sum_{j=1}^{N+1} K_{ij}^k T_j^k + (g_i^k V_i)\right] + \left[1 - \frac{\Delta t}{C_i}\sum_{j=1}^{N+1} K_{ij}^k\right] T_i^k \quad (1)$$

where the thermal transfer coefficient between nodes K_{ij}^k can be obtained by the following equations: (0 for non adjacent nodes),

$$K_{ij}^k = \frac{A_{ij}}{\frac{l_i}{\lambda_i} + R_{\text{cont\_}ij} + \frac{l_j}{\lambda_j}} \quad (2)$$

or

$$K_{ij}^k = \frac{A_{ij}}{\frac{l_i}{\lambda_i} + R_{\text{cont\_an-mem}} + \frac{l_{\text{mem}}}{\lambda_{\text{mem}}} + R_{\text{cont\_mem-cat}} + \frac{l_j}{\lambda_j}} \quad |i \in \text{anode}, j \in \text{cathod} \quad (3)$$

for adjacent nodes, and

$$K_{i\infty} = h_i A_{i\infty} \quad (4)$$

between a surface node and the exterior.

In order to ensure stability of the method, the time interval must be verified:[8]

$$\Delta t \leq \frac{C_i}{\sum_{j=1}^{N+1} K_{ij}^k} \quad (5)$$

For computation of the temperatures of each node at time k $[T(k)]$, it is beneficial to transform the above Eqn (1) to the matrix notation:[8]

$$T(k+1) = MC \cdot [MK \cdot T(k) + MH \cdot T_\infty + MG] + T(k) \quad (6)$$

where

$$MC = \begin{bmatrix} \Delta t / C_1 & 0 & \cdots & 0 \\ 0 & \ddots & \ddots & \vdots \\ \vdots & \ddots & \ddots & 0 \\ 0 & \cdots & 0 & \Delta t / C_N \end{bmatrix} \quad (7)$$

$$MK = \begin{bmatrix} -\sum_{j=1}^{N+1} K_{1j} & K_{12} & \cdots & K_{1(N-1)} & K_{1N} \\ K_{12} & -\sum_{j=1}^{N+1} K_{2j} & \cdots & K_{2(N-1)} & K_{2N} \\ \vdots & \vdots & \ddots & \vdots & \vdots \\ K_{1(N-1)} & K_{2(N-1)} & \cdots & -\sum_{j=1}^{N+1} K_{(N-1)j} & K_{(N-1)N} \\ K_{1N} & K_{2N} & \cdots & K_{(N-1)N} & -\sum_{j=1}^{N+1} K_{Nj} \end{bmatrix} \quad (8)$$

The thermal conductivities between node i and ambient (∞) is:

$$MH = [K_{1\infty} \quad \ldots \quad K_{N\infty}]^t \quad (9)$$

And the thermal generation at node i is:

$$MG = [(g_N^k V_1) \quad \ldots \quad (g_N^k V_N)]^t \quad (10)$$

Although it seems to be a quadratic expression, it can be computed as a linear expression due to the matrix MC being diagonal and that MK has a maximum of seven nonzero values per row and column. This structure significantly reduces the computational time needed by the program.

The channels are included in the matrix representation as isolated nodes with all thermal properties equal to

DOI: 10.1002/apj

zero (literally holes). The heat transfer between the gases and the channel walls ($\dot{q}^k_{\text{ch\_in/out}}$ and $\dot{q}^k_{\text{ch\_aa}}$) is introduced as thermal generation inside the adjacent nodes (to the channels). The thermal generation ($\dot{q}^k_{\text{g}}$) due to the load inside the active area is also introduced as thermal generation inside the adjacent nodes to the active area and distributed between them. The channels in the active area are in contact with their respective gas diffusion layer (3/4 of total surface)and active area (1/4), and the thermal generation due to the reaction is distributed between anode (K_{ga}) and cathode (K_{gc}); this heat is distributed in the model in the following manner:

$$\sum_i g^k_i = \dot{q}^k_{\text{ch\_in/out}} \text{ for nodes in contact with in/out channels.} \quad (11)$$

$$\sum_i g^k_i = \frac{3}{4}\dot{q}^k_{\text{ch\_aa}} \text{ for gas diffusion layer nodes in contact with active area channels.} \quad (12)$$

$$\sum_i g^k_i = \frac{1}{4}\dot{q}^k_{\text{ch\_aa}} + \dot{q}^k_{\text{g}} \text{ for nodes in active area (distributed between anode and cathode).} \quad (13)$$

Heat transfer (thermal generation) at the active area

The quantity of heat generated due to the reaction inside the fuel cell can be evaluated through its higher heating value efficiency, using the following equation:

$$\dot{q}^k_{\text{g}} = \left(\frac{1}{\eta} - 1\right) V \cdot I \text{ where } \eta = \frac{V}{1.482} \quad (14)$$

The heat is assumed to be generated on the cathode active area, while the heat generation from the anode reaction is neglected.[11] In the literature, it is shown that the calculated heat generation due to the reaction is distributed between the anode, membrane and cathode for fully humidified gas streams in a proportion of 3, 4, and 93% respectively.[12]

Heat transfer at the channels and active area due to reactant flows

The heat transfer between the reactant gases and the channel walls is calculated as convection heat exchange inside circular channels for a laminar flow.[8]

It is assumed that both reactants and vapor behave as ideal gases; their partial pressures and/or vapor mass flow can be determined by Dalton's Law

$$\dot{m}_{\text{vap}} = \dot{m}_{\text{H}_2}\frac{M_{\text{H}_2\text{O}}}{M_{\text{H}_2}}\frac{P_{\text{vap}}}{P - P_{\text{vap}}} \text{ and relative humidity is}$$

$$H_{\text{r}} = P_{\text{vap}}/P_{\text{sat}}(T_{\text{in}}) \leq 1. \quad (15)$$

Reactant consumption and water generation can be obtained by the equations

$$\dot{m}_{\text{H}_2\text{\_out}} = \dot{m}_{\text{H}_2\text{\_in}} - \frac{M_{\text{H}_2} I}{2F} \quad (16)$$

$$\dot{m}_{\text{O}_2\text{\_out}} = \dot{m}_{\text{O}_2\text{\_in}} - \frac{M_{\text{O}_2} I}{4F} \quad (17)$$

$$\dot{m}_{\text{H}_2\text{O\_out\_an}} = \dot{m}_{\text{H}_2\text{O\_in\_an}} + K_{\text{wd1}}\frac{M_{\text{H}_2\text{O}} I}{2F} \quad (18)$$

$$\dot{m}_{\text{H}_2\text{O\_out\_cat}} = \dot{m}_{\text{H}_2\text{O\_in\_cat}} + K_{\text{wd2}}\frac{M_{\text{H}_2\text{O}} I}{2F} \quad (19)$$

As stated in Ref. [10], $K_{\text{wd1}} + K_{\text{wd2}} = 1$ and can be determined by the equations shown in Ref. [1, 2].

Gas mixture properties are obtained from the data in NASA database,[13] evaluated at average conditions inside the channel and mixed according to the equations:

$$c_p = \sum_i c_{pi}\frac{\dot{m}_i}{\dot{m}} \quad (20)$$

$$\lambda = \sum_i \lambda_i \frac{\dot{m}_i}{\dot{m}} \quad (21)$$

The heat exchanged between gases and the channel can be obtained by an iterative method, explained in Ref. [8] with equations:

$$h_m = 3.66\frac{\lambda_m}{D} \text{ (for laminar flow)} \quad (22)$$

$$T_{\text{out}} = T_{\text{ch}} + (T_{\text{in}} - T_{\text{ch}}) \cdot \exp\left(\frac{-h_m \cdot \text{Per} \cdot L}{\dot{m}_m \cdot c_{pm}}\right) \quad (23)$$

and

$$\dot{q} = -h_m \cdot L \cdot Per \cdot LMTD \text{ where } LMTD = \frac{T_{\text{out}} - T_{\text{in}}}{\log\left(\frac{T_{\text{ch}} - T_{\text{in}}}{T_{\text{ch}} - T_{\text{out}}}\right)} \quad (24)$$

To this convective heat transfer, the heat generated/absorbed due to the water phase change is added; it can be obtained by the difference between liquid water in and out, and multiplied by the evaporation heat constant of water (h_{v}). Then, heat transfer between the channel and the gases ($\dot{q}^k_{\text{ch\_in/out}}$ and $\dot{q}^k_{\text{ch\_aa}}$) is obtained as the sum of both.

Pressure drop model

The pressure drop in the channel is influenced by the frictional losses in the channel and by the changing channel cross section due to the liquid water. In order to model pressure drop inside the fuel cell, two terms are

DOI: 10.1002/apj

required; the pressure drop produced by the mass flow and a term incorporating liquid water content inside the fuel cell channels.

Pressure drop related to mass flow

The pressure drop inside a channel can be modeled by calculating the major and minor losses, where the first equation depends linearly on mass flow and is modeled by

$$\Delta P_{\text{lin}} = -\frac{57}{\text{Re}}\frac{L}{D}\cdot\frac{\rho_m\cdot v^2}{2} = -\frac{57}{32}\frac{\mu_m}{\rho_m}L\frac{\text{Per}^2}{S^3}\dot{m}_m = -K_{\text{lin}}\frac{\mu_m}{\rho_m}\dot{m}_m \quad (25)$$

and where the second equation depends quadratically on the mass flow and is modeled by

$$\Delta P_{\text{sing}} = -K_{\text{sing}}\frac{1}{\rho_m}\dot{m}_m{}^2 \quad (26)$$

An explanation of these equations can be found in Ref. [9]. Roughly, major losses are associated to pressure drop inside a straight channel, while the minor losses are produced in turns, entrances, and exits and are dependent on empirical data of a given geometry.

Properties of the gas mixtures can be obtained by the equations shown in the section on Thermal Model and the following:

$$\rho = \sum_i \rho_i \quad (27)$$

$$\mu = \frac{\mu_1}{1+\psi_1\frac{M_2}{M_1}} + \frac{\mu_2}{1+\psi_2\frac{M_1}{M_2}} \text{ where } \psi_1 = \frac{\sqrt{2}}{4}\left(1+\left(\frac{\mu_1}{\mu_2}\right)^{0.5}\left(\frac{\dot{n}_1}{\dot{n}_2}\right)^{0.25}\right)^2\left(1+\frac{\dot{n}_2}{\dot{n}_1}\right)^{-0.5} \quad (28)$$

Pressure drop related to liquid water content inside the fuel cell

When there are liquid water droplets present inside the channels, a greater pressure drop is detected in the fuel cell.[14] This extra pressure drop is accounted for in Eqn (26). We believe that this loss is directly associated to a narrowing of the effective cross section of the channels. The amount of restriction is related to the pressure drop induced in the channel due to the flow. The higher the pressure drop, the greater the force that is placed on the upstream side of the water droplet. This force needs to exceed the surface contact resistance of the droplet and that of the channel walls for the droplet to be removed. The dynamics associated with the buildup of water droplets in the channel is not taken into account in this model; however, a steady state constant is determined experimentally for the specific geometry and surface finish of the gas channels.

This effect, at least for the single cell, can be modeled as a special major loss with the equation:

$$\Delta P_W = -K_W\dot{m}_m \quad (29)$$

Combined pressure drop in the case of liquid water inside the fuel cell

According to the previous section, the pressure drop is determined by

$$\Delta P = \Delta P_{\text{lin}} + \Delta P_{\text{sin}\ g} + \Delta P_w = -(K_{\text{lin}}\frac{\mu_m}{\rho_m} - K_w)\dot{m}_m - K_{\text{sing}}\frac{1}{\rho_m}\dot{m}_m{}^2 \quad (30)$$

From Eqn (28) and by comparing it with Eqn (25), it is possible to obtain an approximate equation that models the effective cross section when liquid water appears. It is

$$K_{\text{lin}}\frac{\mu_m}{\rho_m} - K_w = \frac{57}{32}\frac{\mu_m}{\rho_m}L\frac{\text{Per}_{ww}{}^2}{S_{ww}{}^3} \quad (31)$$

If it is assumed that the channel section at active area remains square, even if liquid water is accumulated, then the following equation is obtained.

$$S_{ww}{}^2 = \frac{2}{57}\frac{L}{\left(K_{\text{lin}} - K_w\frac{\rho_m}{\mu_m}\right)} \quad (32)$$

The effective cross section has been found experimentally and is relatively constant for a wide range of operating conditions. Nevertheless, this may be true in the active area of the single cell because the experiments were done with very large stoichiometries; however, in a multicell stack it will require a more complex equation.

APPLICATION OF THE MODEL TO A SINGLE CELL TEST FIXTURE

Single cell test fixture description

The single cell test fixture modeled in this paper is an ElectoChem (model # EFC-05EFC-05-02-02) 5-cm^2 active area fuel cell. It is equipped with a Nafion 115 membrane with 1 mg Pt/cm^2 catalyst loading and Toray carbon fiber paper (Type TGP-H-060) gas diffusion layers, serpentine/straight channel flow field with groups of three channels that come back together at each turn in a uniting manifold. There are five straight

DOI: 10.1002/apj

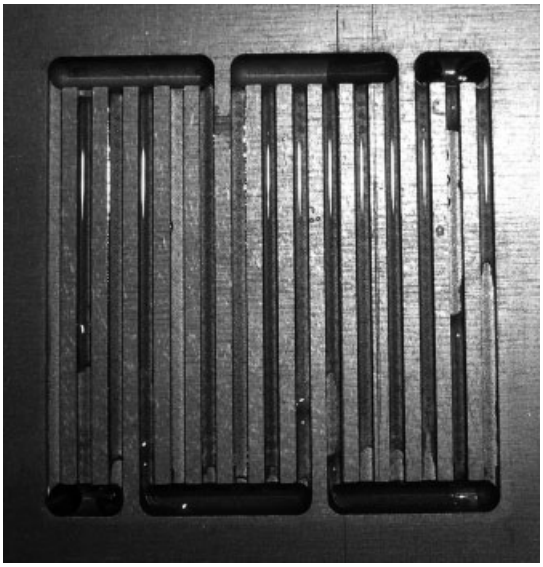

Figure 1. An image of the fuel cell channels configuration.

sections in the flow field, which make it similar to a five pass serpentine configuration, as shown in Fig. 1.

The channels are 0.78 mm wide, 0.78 mm deep, and the space between the channels is 0.78 mm (Table 1). The length of the straight section of a channel is 23.25 mm. The gases enter the flow field through two 1.6 mm diameter holes and exit through holes of the same size. The flow fields are machined into POCO graphite plates that are 19.1 mm thick. The Teflon fitting that connects the fuel cell to the test station is also screwed into the graphite plates. The current collector bus plates are gold-plated copper for enhanced surface conductivity. Resistive square planner 60-W heaters with adhesive are in the center of each bus plate with 50 mm width.

Model assumptions

The following assumptions are made in order to build a reliable, fast, and precise model.

1. One global convection coefficient for the whole cell: With the experimental setup it is impossible to obtain different coefficients for each surface; error committed is low.
2. Physical properties of the materials do not depend on temperature: Temperature range is small (40–80 °C) (Table 2).
3. Calculated properties (c_p, λ, ρ, μ) of dry air do not change very much due to oxygen depletion because of the very high stoichiometry.

Table 1. Dimensional properties of the cell.

		Dimensions					
	Material	x (mm)	y (mm)	z (mm)	Volume (m^3)	Convective area (m^2)	Contact area (m^2)
Heating sides	–	–	–	–	–	1.06E-02	–
Heaters	–	–	50.0	50.0	–	–	2.50E-03
Copper plates	Copper	3.3	95.5	111.0	3.50E-05	2.56E-03	9.09E-03
Graphite plates	graphite	19.35	95.5	95.2	1.76E-04	5.53E-03	9.09E-03
Diffusion layer	carbon paper	0.28	22.4	22.4	1.40E-07	–	5.00E-04
Gasket	Silicon	0.28	–	–	2.41E-09	–	8.59E-03
Membrane	NAFION	0.15	95.5	95.2	1.36E-06	–	9.09E-03
Lab. support	Acrylic	46.01	95.5	10.0	4.39E-05	4.39E-03	–

Table 2. Thermal properties of the cell.

	Thermal/physical properties		
	ρ density (kg/m^3)	c_p specific heat [J/(K·Kg)]	λ thermal conductivity [W/(m·K)]
Heating sides	–	–	–
Heaters	–	–	–
Copper plates	8954	384	395
Graphite plates	2200	980	120
Diffusion layer	1500	400	1.7
Gasket	710	440	0.4
Membrane	–	–	0.35
Lab. support	1460	1190	0.2

DOI: 10.1002/apj

4. Properties of the flow inside the active area are determined for the average mass flow between entrance and exit.
5. Ideal gases are assumed.
6. It is assumed that $K_{wd1} = 0.3$ and $K_{wd2} = 0.7$; these constants have little effect on the simulations due to the high stoichiometries.
7. The channels in the active area are modeled as 3-parallel long straight tubes. This reduces precision and computational time. For a small single cell this assumption can be made.
8. No heat transfer by radiation: low temperature, nonlineal equation (thermal model is lineal); the determined convection coefficient includes radiation at a given temperature.

Fuel cell mesh

The mesh applied in the model of the single cell is shown in Fig. 2. It divides the different zones of the cell with the corresponding materials. Smaller cuboids are placed in the active area for higher precision.

Properties of the materials

Most of the constants were obtained from material suppliers, fuel cell supplier, or different reference books. They can be found in Tables 1 and 2.

EXPERIMENTAL METHODOLOGY

In this section we present the single cell test fixture, the experimental setups, and the LabView hardware and software used for data acquisition.

Experimental setup

The test station consists of two reactant (anode and cathode) gas subsystems. Each subsystem contains a Bronkhorst mass flow controller, membrane-based humidification with dew point sensors for control, inlet line heaters to prevent condensation, absolute pressure transducers at the inlet, differential pressure transducers between the inlet and outlet of each reactant, and back pressure regulator at the outlet of the fuel cell to control system pressure. The mass flow controllers are each calibrated for the specific gas (hydrogen for the anode and synthetic air for the cathode).

There are eight temperature sensors that come from the fuel cell by way of K type thermal couples. Four of the measurements are of the graphite plates (two in each plate) with one connected to a RedLion PID controller model #T4810105 that controls the temperature of the fuel cell. The cooling of the cell is attained mainly by natural convection. The other four temperature measurements are of the reactants inlets and outlets. The inlet temperature measurements are close to the outlet of the gas line heaters but still outside the cell. The outlet temperatures are measured inside the fuel cell in the outlet manifold. All the measurement and control are made in real time through LabView and are explained in more detail in the following section.

Two computers are used to define the data acquisition and control system. The first one is responsible for the user interface and in setting the operating conditions. This is done by means of a graphical interface developed by our laboratory through LabView. The second computer runs under a Real Time Operating System (RTOS) which works in deterministic mode offering consistent and stable functionality for

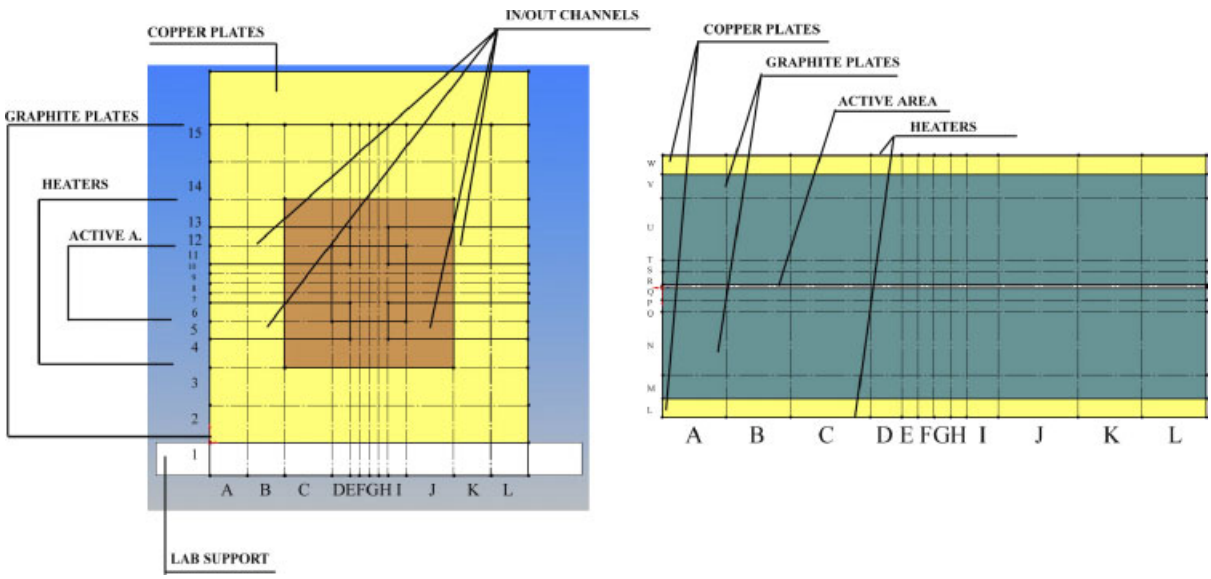

Figure 2. Single cell mesh. This figure is available in colour online at www.apjChemEng.com.

DOI: 10.1002/apj

the implementation of controllers and to store the data. Inside a RTOS computer, there are CompactRIO cards with input/output modules that contain configurable signal conditioning, isolation, and screw terminals to provide direct connections to our sensors and actuators.

Experiments for parameter identification and verification

In order to adjust some unknown parameters such as global convective coefficient, internal contact resistances, and pressure drop constants to become known, and to verify the model, several experiments were performed, and simulated with the model (Fig. 3). These experiments were designed based on the data acquisition components and the fuel cell active area. All parameters were adjusted following a 'minimum global error' strategy.

The first set of experiments was designed to obtain the thermal constants (global convective coefficient and internal contact resistances) and check the thermal model (Tables 3 and 4). All of them were done without reactant flows. These experiments are divided into six groups:

- The flow of heaters current is adjusted in order to reach a thermal equilibrium inside the cell. This is done to calculate and verify the convection heat transfer parameter of the cell.
- The cell is heated using both heaters (no equilibrium is reached). This is done to calculate and verify convection parameter and heat capacity of the cell.
- The cell is cooled (no refrigeration system; no equilibrium is reached). This is done to verify all the previously stated parameters.
- The cell is heated using only one heater and the current flow is adjusted to reach thermal equilibrium inside the cell. This is to calculate and verify the convection parameter and internal contact resistances.
- The cell is heated with only one heater at maximum current (no equilibrium is reached). This is to verify all the previously stated parameters under different conditions.
- A temperature profile is followed turning the heaters on and off. This is done to verify all the previously stated parameters.

The adjusted parameters are given in Table 3.:

The second set of experiments was designed to check pressure drop inside the cell (Table 5), all of them were done with H_2/air, at different flow rates (0.5–1.5 SLPM), at different dew point and cell temperatures (30–80 °C), different currents (0–5 A), and with/without water condensation. It was impossible to work with low flow rates due to the extremely low pressure drops. Most of the experiments were done with flow rate 1.5 SLPM on both sides.

SELECTED RESULTS FOR THE SINGLE CELL TEST FIXTURE

This section presents selected results for the 2D temperature distribution snapshot as well as the temperature evolution in the cell.

Table 3. Thermal properties of the cell (adjusted).

	R_{ij} contact resistance ($W \cdot m^2/K$)	h convectivity ($W/(m^2 \cdot K)$)
Heating sides	–	12
Heaters	–	–
Copper plates	Copper–graphite 0	12
Graphite plates	Graphite–diffusion layer 0.00045	12
Diffusion layer	Dif. layer anode–membrane 0.00045	–
Gasket	Dif. layer cathode–membrane 0.00045	–
Membrane	–	–
Lab. support	–	9.23

Table 4. Heat balance for several experiments.

All measurements taken at two different temperature points	Two heaters: thermal equilibrium		Two heaters: full power		Two heaters: 1/4 power		One heater: thermal equilibrium	One heater: full power		No heaters	
$P_{heaters\_real}$ (W)	−15.12	−16,38	−100.28	−100.28	−28.50	−28.50	−16.38	−51.24	−51.24	0.00	0.00
P_{conv_mod} (W)	15.90	18.02	14.03	23.21	12.11	14.67	17.47	3.75	15.46	11.82	16.43
P_{stored_mod} (W)	0.00	0.00	95.32	67.28	13.29	12.37	0.00	51.66	36.10	−14.59	−15.82
Error (W)	0.78	1.64	9.07	−9.79	−3.10	−1.46	1.09	4.17	0.31	−2.77	0.62

DOI: 10.1002/apj

Table 5. Pressure drop constants (adjusted).

	H_2	Air
K_{lin} (s^2/m^3)	3.7×10^{12}	9×10^{12}
K_{sing} ($Pa \cdot s^2/kg \cdot m^3$)	1.8×10^{12}	1.9×10^{12}
K_w (Pa·s/kg)	2.8×10^7	7.5×10^7

The comparison between acquired data and simulated with the Matlab model is shown in Figure 3.

Temperature distribution inside the fuel cell at a fixed time

Figures 4–6 show the temperature distribution across the fuel cell and the change in the inlet and outlet reactant temperatures at a given time where every rectangle represents the temperature of a cuboid. This corresponds to a small fuel cell where the majority of the heat comes from two contact resistances, one on each side. It is critical to determine the thermal distribution because of its relationship with the phase change of water.

Evolution of fuel cell temperature over time

The model simulates the evolution over time of every cuboid temperature and temperature of the reactant. This allows for the simulation of nonequilibrium temperature pattern in the fuel cell. Figure 7 shows the temperature evolution through time, at a fixed location in the fuel cell while the heaters are cycled on and off.

Figure 8 shows relative humidity of the gases and liquid water content, through the anode and cathode. These illustrations are important in order to determine if and where water is condensing inside the fuel cell, which is a key factor in fuel cell efficiency and stability. In this case, on the anode side the hydrogen reaches its saturation temperature at the first node entering the fuel cell and starts condensing; however, on the cathode side the air reaches its saturation temperature at the third node.

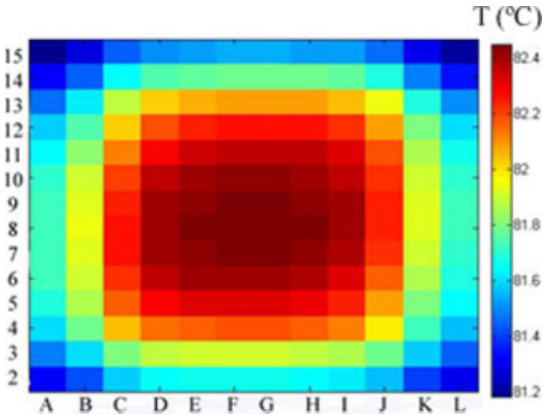

Figure 4. Longitudinal cut of the cell. This figure is available in colour online at www.apjChemEng.com.

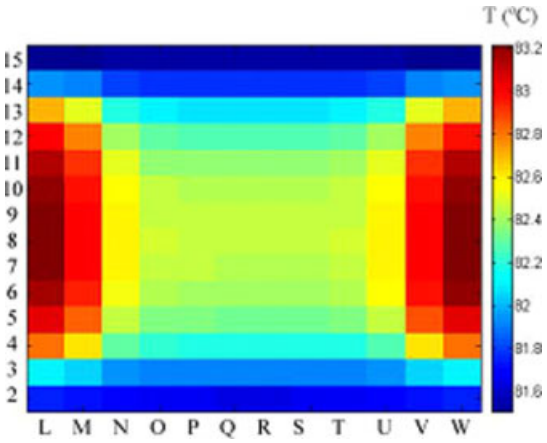

Figure 5. Transversal cut of the cell. This figure is available in colour online at www.apjChemEng.com.

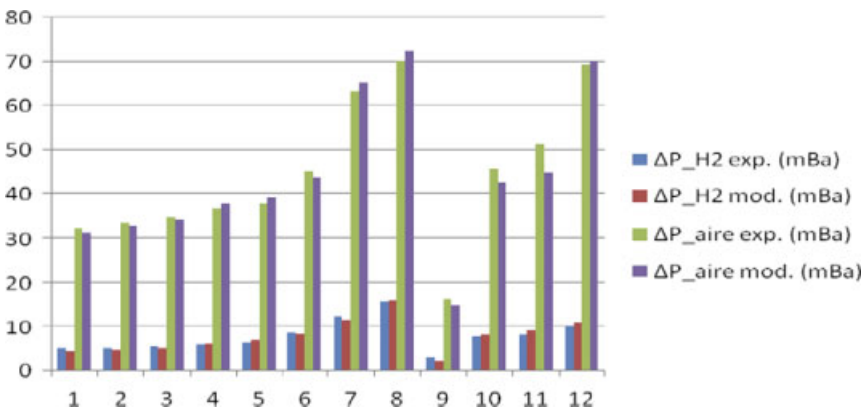

Figure 3. Pressure drop comparison of experimental data with simulated data. This figure is available in colour online at www.apjChemEng.com.

DOI: 10.1002/apj

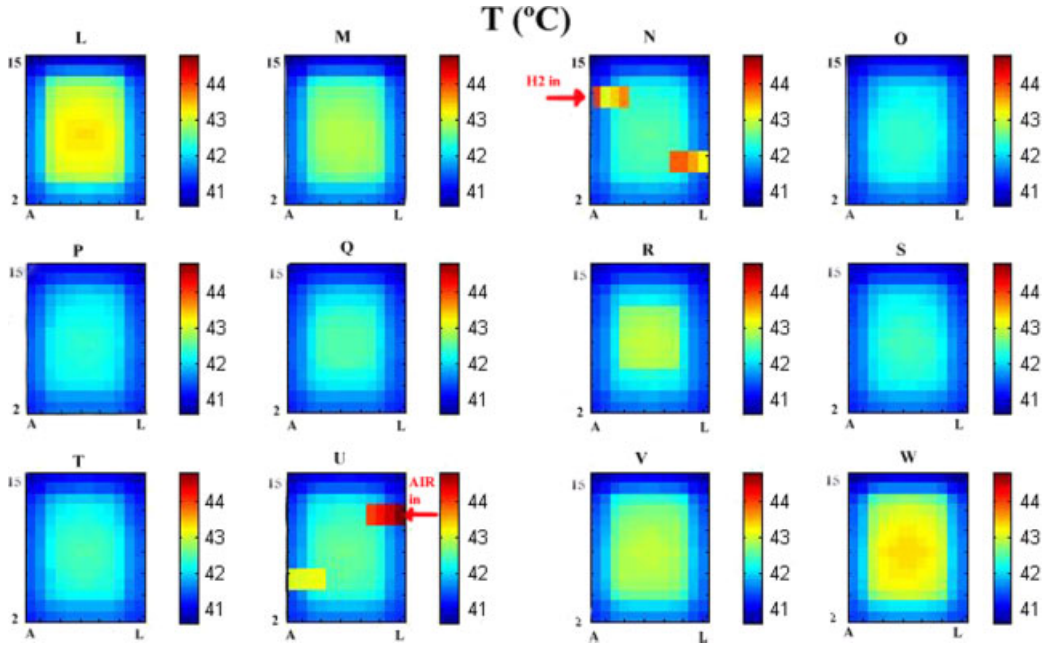

Figure 6. Longitudinal cuts through the cell at a given time. This figure is available in colour online at www.apjChemEng.com.

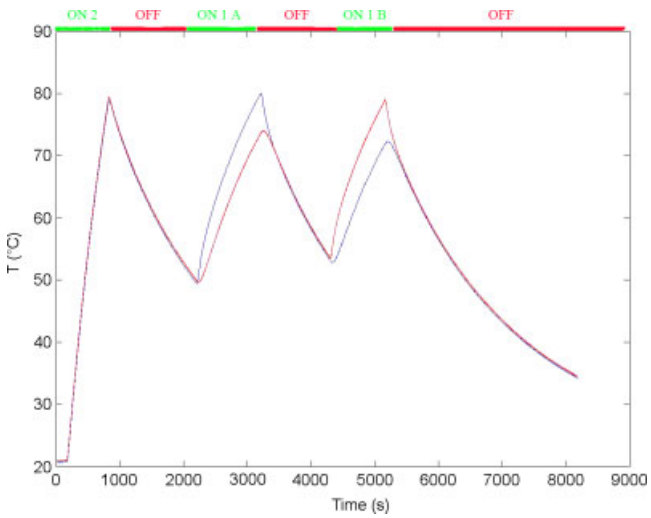

Figure 7. Temperature evolution with respect to time at two fixed points in the fuel cell. One in the anode side and one in the cathod side. This figure is available in colour online at www.apjChemEng.com.

Figure 9 shows the current at which water condenses inside the active area (critical current), for different temperatures and flow rates. Any point above each line will result in condensation in the flow field at the given conditions. Raising the current while all the other parameters remain constant will eventually lead to water condensation inside the active area. This model is designed to determine this critical maximum current.

Figure 10 shows the pressure drop in the channels for a fixed flow rate and the difference in temperature between the fuel cell and dew point while modifying the current. The discontinuity corresponds to the critical current. The simulation shows the sensitivity of condensation of water with respect to fuel cell and dew point temperatures, current, and flow rates. A one-degree change in the temperature difference greatly affects the critical current. Increasing overall temperature increases the capacity of the gases to remove water in the vapor form which, in turn, increases the critical current.

Figure 11 shows the pressure drop for the reactant gases with a fixed stoichiometry and temperature versus modifying the current. Increasing the current implies increasing the flow rate, which provokes a greater pressure drop inside the cell. It can be seen that both dew point temperature and stoichiometry have a great effect on the pressure drop. This is due to the quantity of water added to the cell.

CONCLUSIONS

In this work, a three-dimensional model of heat distribution and pressure drop for PEMFC was developed and experimentally tested. It includes a simple two-phase flow pressure drop model that is representative of the true effects of liquid water in the flow field. The model is especially suited for the analysis of liquid water condensation in the reactant channels.

The model was applied to a single cell test fixture and some of the parameters were adjusted through a series of experimental tests. The model was validated using experiments designed for this purpose. The

DOI: 10.1002/apj

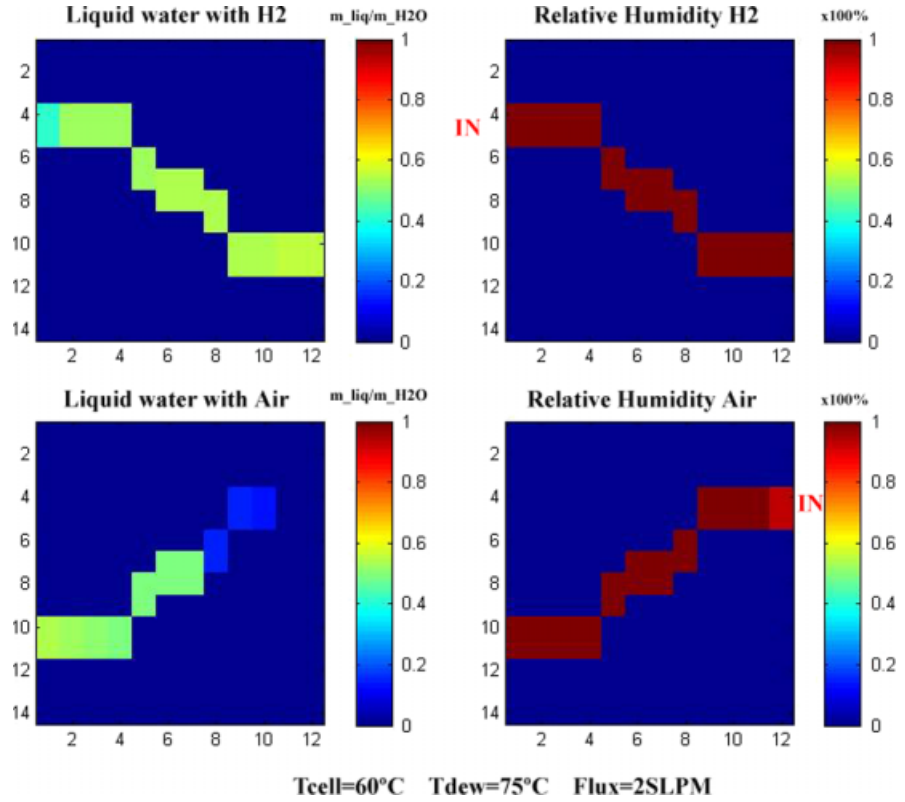

Figure 8. Relative humidity and liquid water content of the reactant gases through the cell. This figure is available in colour online at www.apjChemEng.com.

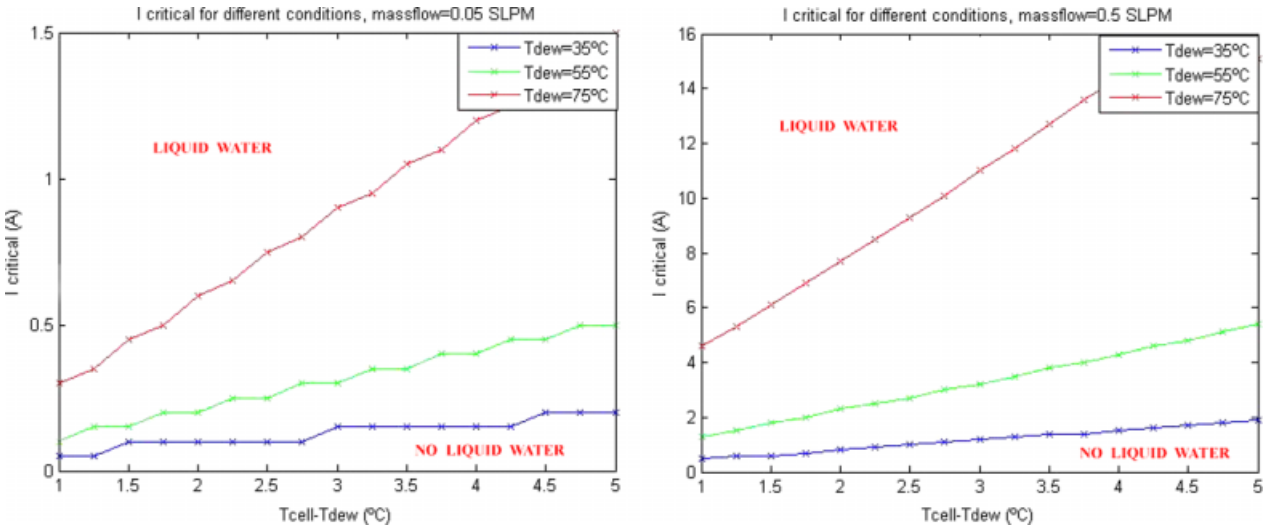

Figure 9. Critical current with respect to ΔT between fuel cell and reactant dew point. This figure is available in colour online at www.apjChemEng.com.

identified parameters are contact resistances, convective heat transfer coefficients, and pressure drop constants.

Several simulations were performed and analyzed. The results show that there is a step jump in the pressure drop when the critical current is reached. This determines the maximum current that should be applied to the fuel cell to avoid flooding of the catalyst layers and diffusion layers. Critical currents and the effects of liquid water and water vapor on the pressure drop of the fuel cell were evaluated for a range of operating conditions. The model shows that the current at which water condenses inside the reactant channels (or critical current) depends strongly on the flow rate and even more

DOI: 10.1002/apj

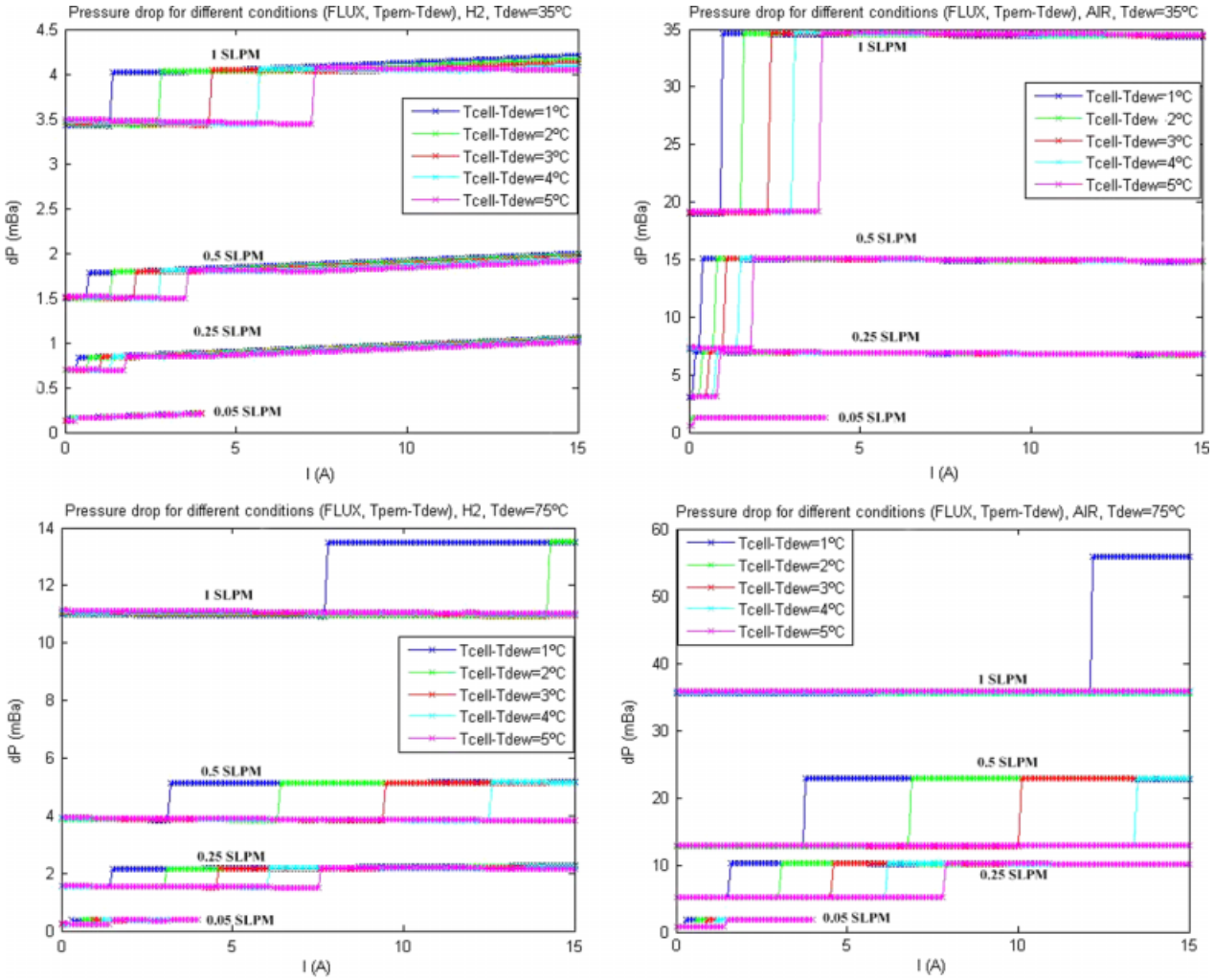

Figure 10. Pressure drop against current, fixed mass flow. This figure is available in colour online at www.apjChemEng.com.

on the temperature difference between the fuel cell and the reactant dew point. The model also shows that lower overall temperature gives a smaller critical current.

FUTURE WORK

Improvements in future versions of the model are the following:

- To apply the model to a fuel cell stack.
- to introduce more complex equations to model the pressure drop inside the cell. To achieve it, it is necessary to apply the model to a fuel cell (not single cell) with higher pressure drops and lower stoichiometry in order to have a greater range of possible experiments. For the operating range of the single cell in the lab, it has been confirmed that this simple model is quite enough.
- to introduce more complex equations to model water movements inside the active area. Once again, that will be necessary when modeling a fuel cell stack. As a reference, these equations can be found at Ref. [2].
- to introduce an electrical model, it is to say, a submodel which determines cell voltage at working conditions.

The following are some of the future objectives of research that will be conducted with more lab experiments and aids of models.

- To determine the quantity of liquid water that remains inside the cell dynamically and in steady state.
- To determine or verify the water movements inside the active area. It is related to figure 10.
- Create a more universal and precise approximation of section reduction due to liquid water formation inside the cell.

DOI: 10.1002/apj

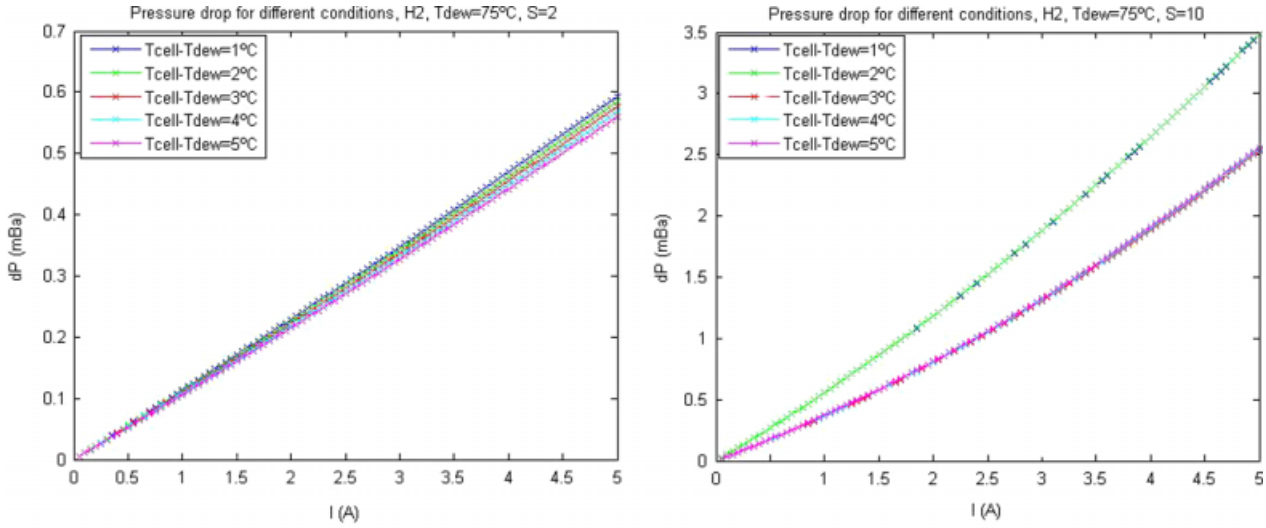

Figure 11. Pressure drop against current, fixed stoichiometry (analog for Air). This figure is available in colour online at www.apjChemEng.com.

Acknowledgements

This work has been funded partially by the projects CICYT DPI2007-62966 and CICYT DPI2004-06871-C02-01 of the Spanish Government.

MODEL AND CONTACT

The implementation in Matlab/Simulink of the model for the single cell used in our laboratory can be found at the following address:http://wikiri.upc.es/wiki/

NOMENCLATURE

A_{ij}	Contact area between nodes i and j (m^2)
c_{p_i}	Thermal capacity of fluid i (J/kgK)
c_{pm}	Thermal capacity of the flow at average conditions (J/kgK)
C_i	Thermal capacity of node i, $C_i = \rho_i V_i c_i$ (J/K)
c_i	Thermal capacity of node i (J/kg K)
D	Channel hydraulic diameter (m)
F	Faraday constant 96485 (C/mol)
g_i^k	Heat generated in node i at time k(W/m^3)
h_i	Convection coefficient of node i (W/m^2K)
h_m	Convection coefficient of the flow, evaluated at average conditions (W/m^2K)
H_r	Relative humidity of the flow
I	Fuel cell current (A)
K_{ij}^k	Thermal transfer coefficient between nodes i and j at discrete time k (W/mK)
K_{wd1}	Quantity of generated water going into the H_2 side
K_{wd2}	Quantity of generated water going into the air side
K_{lin}	Major pressure drop dimensional constant ($1/m^3$)
K_{sing}	Minor pressure drop dimensional constant ($1/m^4$)
K_{w}	Pressure drop constant due to liquid water (1/ms)
K_{ga} (K_{gc})	Percentage of total heat generation due to the reaction, produced in anode (cathode)
l_i	Width of node i in the axis perpendicular to contact area between nodes i and j (subindex mem for membrane) (m)
L	Channel length (m)
$\dot{m}_{xx}$	Mass flow of fluid xx (kg/s)
$\dot{m}_m$	Mass flow of gases at average conditions (kg/s)
M_{xx}	Molar mass of element xx (g/mol)
$\dot{n}_i$	Molar flux of fluid i (mol/s)
P_{xx}	Partial pressure of fluid xx (Pa)
P	Total pressure of gases (Pa)
$P_{\text{st}}(T_{\text{in}})$	Saturation pressure of water at temperature T_{in}
ΔP_{lin}	Pressure drop due to major losses (Pa)
ΔP_{sing}	Pressure drop due to minor losses (Pa)

ΔP_{w}	Pressure drop due to liquid water inside channel (Pa)
Per	Channel hydraulic perimeter (m)
Per_{ww}	Effective channel hydraulic perimeter with liquid water (m)
$\dot{q}^k_{\mathrm{ch\_in/out}}$	Heat transfer between gases and in/out channel walls (W)
$\dot{q}^k_{\mathrm{ch\_aa}}$	Heat transfer between gases and active area channel walls (W)
$\dot{q}^k_{\mathrm{g}}$	Thermal generation inside the active area due to the reaction (W)
R_{cont_ij}	Contact thermal resistance between nodes i and j ($\mathrm{Wm^2/K}$)
$R_{\mathrm{cont\_an-mem}}$ and $R_{\mathrm{cont\_mem-cat}}$	Contact thermal resistance between anode and membrane (membrane and cathode respectively) ($\mathrm{Wm^2/K}$)
S	Channel cross section ($\mathrm{m^2}$)
S_{ww}	Effective channel cross section with liquid water ($\mathrm{m^2}$)
T^k_i	Temperature of node i (for $i = 1 \ldots N$, where N equals the number of cubes inside the mesh), at time k (K)
$T = (T_1 \ldots T_N)^t$	Vector of nodal temperatures
T_{out}	Gas temperature out (K)
T_{ch}	Temperature of the nodes in contact with gases (K)
T_{in}	Gas temperature in (K)
Δt	Time elapsed between instants k and $k+1$ (s)
V_i	Volume of the cube represented by node i ($\mathrm{m^3}$)
V	Voltage given by the fuel cell (V)
v	Velocity of the gas (m/s)
λ_i	Thermal conductivity of fluid i of the flow or thermal conductivity of node i (subindex mem for membrane) (W/mK)
λ_m	Thermal conductivity of the gases at average conditions (W/mK)
η	Fuel cell efficiency
ρ_i	Density of fluid i of the flow or density of node i, what corresponds ($\mathrm{kg/m^3}$)
ρ_m	Density of the gas at average conditions ($\mathrm{kg/m^3}$)
ρ	Density of the gas ($\mathrm{kg/m^3}$)
μ_i	Viscosity of fluid i (Pa·s)
μ	Viscosity of the gas (Pa·s)
∞	Subindex, represents ambient node

REFERENCES

[1] T.E. Springer, T.A. Zawodzinski, S. Gottesfeld. *J. Electrochem. Soc.,* **1991;** *138*(8), 2334–2342.
[2] T.V. Nguyen, R.E. White. *J. Electrochem. Soc.,* **1993;** *140*(8), 2178–2186.
[3] K. Broka, P. Ekdunge. *J. Appl. Electrochem.,* **1997;** *27*(3), 281–289.
[4] M. Coppo, N.P. Siegelb, M.R. Von Spakovskyc. *J. Power Sources,* **2006;** *159*(1), 560–569.
[5] D.M. Bernardi, M.W. Verbrugge. *J. Electrochem. Soc.,* **1992;** *139*(9), 2477–2491.
[6] Y. Shan, S.Y. Choe. *J. Power Sources,* **2005;** *145*(1), 30–39.
[7] S. Um, C.Y. Wang. *J. Power Sources,* **2006;** *156*(2), 211–223.
[8] F.P. Incropera, D.P. DeWitt. *Introduction to Heat Transfer*, Wiley, New York: **1996**.
[9] F.M. White. *Fluid Mechanics*, McGraw-Hill, New York: **1999**.
[10] F. Barbir. *PEM Fuel Cells: Theory and Practice*, Elsevier Inc., New York: **2005**.
[11] M.J. Lampinen, M. Fomino. *J. Electrochem. Soc.,* **1993;** *140*(12), 3537–3546.
[12] H. Ju, H. Meng, C.Y. Wang. *Int. J. Heat Mass Transfer,* **2005;** *48*(7), 1303–1315.
[13] A. Burcat, B. Ruscic. *Third Millennium Ideal Gas and Condensed Phase Thermochemical Database for Combustion*, Technical Report Argonne National Lab, Chicago: **2005**.
[14] F. Barbir, H. Gorgun, X. Wang. *J. Power Sources,* **2005;** *141*(1), 96–101.
[15] L. You, H. Liu. *Int. J. Heat Mass Transfer,* **2002;** *45*(11), 2277–2287.
[16] V. Gurau, H. Liu, S. Kakaç. *AIChE J.,* **1998;** *44*(11), 2410–2422.